Acta Geotechnica
https://doi.org/10.1007/s11440-023-02204-9

SHORT COMMUNICATION

Numerical investigation of the instability of dry granular bed induced by water leakage

Nhu H. T. Nguyen[1] · Thanh T. Nguyen[2]

Received: 2 April 2023 / Accepted: 17 December 2023

Abstract
Underground pipe defects or cracks under transport infrastructure can cause water leakage to upper soil layers (e.g. subgrade and capping), inducing local cavities or even failure of overlying road/railway formation. Although numerous studies on the instability of granular beds induced by injected water have been conducted, most of them focused on the behaviour of saturated granular beds, while research on dry granular beds is still limited. This paper aims to address this gap using a numerical model coupling volume of fluid method with discrete element method. We observed that dry granular beds go through three distinct regimes as water jet velocity increases including stationary, stable deformation with heave and fluidisation. However, the flow velocities required to deform and fluidise dry granular beds are significantly higher than those required for saturated beds. Increasing granular bed thickness can alter its failure mechanism from full depth to localised erosion, leading to cavity formation around pipe cracks prior to the bed fluidisation. The gravitational and frictional components of granular mass are identified as two main resisting forces of dry granular beds against water jet force, evidenced by the increase of critical jet velocities as particle density and friction coefficient increase. Nevertheless, the moblised zone of granular mass is practically independent of both the buried depth of dry granular beds.

Keywords Erosion · Granular bed · Pipe leakage · Soil fluidisation · VOF-DEM · Water jet

1 1 Introduction

Underground pipe networks play a vital role in urban development to transport water and sewage. Pipe defects or cracks are one of the most common incidents occurring during their service life. For example, many pipes crossing under roads and railways can experience significant impacts due to traffic loads, resulting in damages with water leakage. Water exfiltration through defective pipes can erode soil particles in upper soil bed, leading to cavity formation and failure of entire bed under roads and urban infrastructure (see Fig. 1). This problem often occurs at a large scale, causing considerable challenges to investigate the bed stability in response to water exfiltration. Researchers rather used downscale models of upward water jet beneath a soil bed to study this problem. For instance, Zoueshtiagh and Merlen [32] conducted a series of experiments to investigate the effects of punctual water jet on a submerged granular bed and found that the bed exhibits three distinct regimes: static, constant deformation and fluidisation, associated with increasing values of injected flow rate. Alsaydalani and Clayton [2] used a plane-strain experimental model to assess the deformation of saturated soil beds induced by injected water. They revealed the effects of various factors including particle size and shape, burial depth and orifice size on the bed behaviour. Recently, Jiang et al. [11] developed a 3D experiment using transparent soil to observe the evolution of cavity in response to increasing flow rate. They found that soil with larger particle size and lower porosity would improve the bed stability against upward water jet, thereby suggesting the use of coarse and dense soil for pipe backfill as well as interactive regions with road foundation.

✉ Nhu H. T. Nguyen
nhu.nguyen@deakin.edu.au

[1] School of Engineering, Faculty of Science, Engineering and Built Environment, Deakin University, Waurn Ponds, VIC 3216, Australia

[2] Transport Research Centre, School of Civil and Environmental Engineering, University of Technology Sydney, Ultimo, Australia

Published online: 08 February 2024

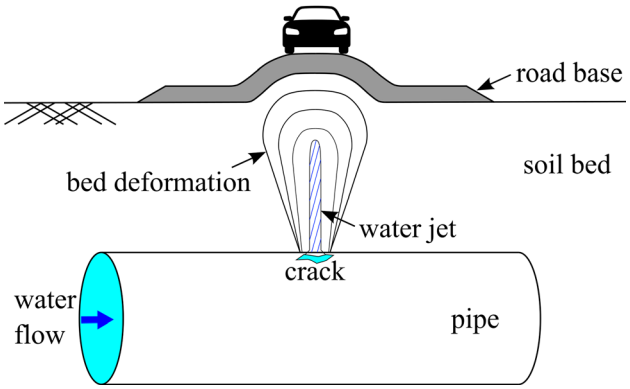

Fig. 1 Illustration of the instability of soil bed under a road base induced by water jet from pipe crack

Alongside experiments, several numerical methods have also been applied to investigate this problem including the coupled discrete element method (DEM) and lattice Boltzmann method [5, 20] or computational fluid dynamics (CFD) [25]. These coupling methods have advantages in providing insights into systems involving particle–fluid interactions which underpin a wide range of geotechnical problems relevant to granular materials [29]. Since being first developed, significant advancements have been made on these methods to facilitate their engineering applications such as the description of interactions between fluid and irregular particle shapes (e.g. [7, 30]) and multiphase fluid flow (e.g. [15, 23]).

Although the above experimental and numerical studies provided significant insights into the instability of granular beds induced by water jet, they focused merely on submerged or (partially) saturated granular beds, while the behaviour of dry granular beds subjected to water leakage was still overlooked despite its common occurrence in practice. An example of this problem is the collapse of overlying soil induced by shallow pipe burst where the soil is well above the groundwater level, causing damage to road infrastructure and traffic incidents (e.g. [18, 24]). To draw appropriate attention to this problem, in this study, we investigate the behaviour of dry granular beds under the effects of injected water using a numerical method coupling volume of fluid (VOF) and DEM. The combination of VOF and DEM enables the description of interactions between free-surface fluid (i.e. water jet) and dry particles, making it particularly suitable for this problem. The numerical model is first validated against the experiment of dry spout beds. Numerous simulations are then conducted to investigate the behaviour of dry granular beds subjected to an upward water jet to represent water burst through a pipe crack, and the effects of several parameters including granular bed thickness, inlet size and material properties on the bed instability. Our main focuses through this short communication are to highlight the distinctions between the behaviours of dry and saturated granular beds against water jet and identify key influencing factors that need to be considered in the bed stability assessment.

2 2 Theoretical background and model establishment

The current study adopted the VOF-DEM coupling method to simulate dry granular beds subjected to water jet. This section briefly summarises the main formulations of this method followed by numerical setup to verify and investigate the behaviour of dry granular beds subjected to upward water jet.

2.1 Theoretical background of the VOF-DEM method

2.1.1 VOF formulations

In the VOF-DEM coupling method, the multiphase fluid is described by VOF, which is an Eulerian approach for simulating multiphase fluid flow. The formulation of VOF method is essentially an extension from the conventional CFD governing equations to incorporate multi-fluids volume fractions and a surface tension model to describe their interface evolution. To model multiphase fluid flow with a single set of governing equations, the volume-weighted average of fluid densities (ρ_f) and dynamic viscosities (μ_f) are first defined as $\rho_f = \sum_{i=1}^{n} \alpha_i \rho_{fi}$ and $\mu_f = \sum_{i=1}^{n} \alpha_i \mu_{fi}$, where i denotes each fluid in the multiphase system (e.g. water and air) and α_i is its volume fraction. The governing equations and volume fraction evolution of VOF method are expressed as follows:

$$\frac{\partial \epsilon}{\partial t} + \nabla.(\epsilon \boldsymbol{u}_f) = 0 \tag{1}$$

$$\frac{\partial \epsilon \rho_f \boldsymbol{u}_f}{\partial t} + \nabla.(\epsilon \rho_f \boldsymbol{u}_f \boldsymbol{u}_f) = -\epsilon \nabla p + \epsilon \nabla.\boldsymbol{\tau} + \epsilon \rho_f \boldsymbol{g} + \epsilon \boldsymbol{F}^{\sigma} + \boldsymbol{F}^{\text{drag}} \tag{2}$$

$$\frac{\partial \epsilon \alpha_i}{\partial t} + \nabla.(\epsilon \alpha_i \boldsymbol{u}_f) - \nabla.[\boldsymbol{u}_c \alpha_i (1 - \alpha_i)] = 0 \tag{3}$$

where $\boldsymbol{u}_f$ is the fluid velocity; $\boldsymbol{u}_c$ is the compression velocity; p is the fluid pressure; $\boldsymbol{\tau}$ is the Newtonian fluid stress tensor; ϵ is the void fraction; $\boldsymbol{g}$ is the gravity; F^{σ} is the surface tension force, which is described by a surface tension force model [3]; and $\boldsymbol{F}^{\text{drag}}$ is the volume average of drag forces of fluid acting on particles. The drag forces, in turn, are described by a drag force model. In this study, we adopted Koch and Hill drag force model [14], which has

been demonstrated to reasonably capture the behaviour of multiphase fluid-particle systems [21, 27].

2.1.2 DEM formulations

The solid particle phase, on the other hand, is modelled by DEM which describes particle motion in accordance with Newton's second law as follows:

$$m_i \frac{\mathrm{d}\boldsymbol{u}_{\mathrm{p},i}}{\mathrm{d}t} = \boldsymbol{F}_i^{\mathrm{pp}} + \boldsymbol{F}_i^{\mathrm{pf}} + m_i \boldsymbol{g} \tag{4}$$

$$\mathrm{I_i} \frac{\mathrm{d}\boldsymbol{\omega}_{\mathrm{p},i}}{\mathrm{d}t} = \boldsymbol{M}_i^{\mathrm{pp}} \tag{5}$$

where m_i and I_i are the mass and moment of inertia of particle i; $u_{\mathrm{p},i}$ and $\omega_{\mathrm{p},i}$ are its translational and angular velocity, respectively; F_i^{pp} and M_i^{pp} are the total interaction force and rotational torque acting on this particle; and F_i^{pf} is the particle–fluid interaction force. In this study, the particle–particle interaction force is described by the Hertz-Mindlin contact model [6, 10, 19] with added rolling friction characterised by a directional torque contact model [1, 31]. The fluid-particle interaction force comprises four main components: drag force, pressure gradient force, viscous force and surface tension force, i.e.

$$\boldsymbol{F}_i^{\mathrm{pf}} = \boldsymbol{F}_{\mathrm{drag},i} + \boldsymbol{F}_{\nabla \mathrm{p},i} + \boldsymbol{F}_{\tau,i} + \boldsymbol{F}_{\sigma,i} \tag{6}$$

where $F_{\mathrm{drag},i}$ is the drag force acting on particle i determined by the drag force model; $F_{\nabla \mathrm{p},i} = -V_{\mathrm{p},i}\nabla p$ is the pressure gradient force; $F_{\tau,i} = V_{\mathrm{p},i}\nabla \cdot \tau$ is the viscous force; $F_{\sigma,i} = V_{\mathrm{p},i}F^{\sigma}$ is the surface tension force and $V_{\mathrm{p},i}$ denotes the volume of particle i.

2.2 Model verification

The coupling between VOF and DEM is based on the four-way coupling algorithm [13] and was implemented into the open-source CFDEM code [27], which combines LIGGGHTS (DEM) code and OpenFOAM multiphase (fluid) solver. The VOF-DEM method has been successfully applied in previous studies to model systems involving particles motion and free-surface fluid flows (e.g. [21, 22, 27]). In order to further verify its applicability to model the instability response of dry granular bed under fluid jet force, we simulate the spout fluidised bed test under pressurised air flow [17], which is a common test to examine the fluidisation behaviour of particle assemblies. Numerical results are then benchmarked with the experimental counterparts. It is worth noting that there is practically no appropriate experiment of dry granular bed instability subjected to water jet that we can find in the literature. Thus, the spout fluidised bed test with similar mechanisms such as the local channel formation followed by fluidisation of the entire particle beds under increasing jet force was chosen for the model verification.

The schematic representation of the spout fluidised bed test is given in Fig. 2. The bed domain is a box of 154 × 1000 × 84 mm. The bed is filled with 44,800 glass particles with the diameter of 4 mm and density of 2,526 kg/m^3. During the testing process, pressurised air is injected into the bed through a rectangular gauze of 22 × 12 mm located at the bed bottom near the front side. The spout velocity is gradually increased from 40 to 90 m/s with an increment of 5 m/s. In the VOF-DEM model, the pressurised air and atmospheric air are simulated by two different fluid phases. The density and kinematic viscosity of pressurised air are 1.2 kg/m^3 and 1.5 × 10^{-5} m^2/s, respectively, which are chosen according to previous studies of spout beds with similar setups [12, 28]. The coefficients of sliding and rolling friction between particles in this simulation are 0.1, as per the value used in the simulations of glass beads performed by Goniva et al. [8]. The use of such low inter-particle friction coefficients as compared to those generally used in the simulations of geomaterials is attributed to that glass beads have much smoother surface than geomaterials like sands or gravels. Goniva et al. [8] also demonstrated in their study that DEM simulation of the angle of repose test with the friction coefficient of 0.1 produced similar results as the experiment of glass beads with the resulting angle of repose being around 20 degrees.

The simulation results reveal that under the effects of increasing the spout velocity, the bed behaviour switches from a stationary regime with no significant movement of particles to an internal spouting regime where a spout channel gradually develops upwards, forming a local cavity under the bed surface. Figure 3a compares the experimental and numerical results at a time instance with the spout velocity of 75 m/s. They both show that the spout

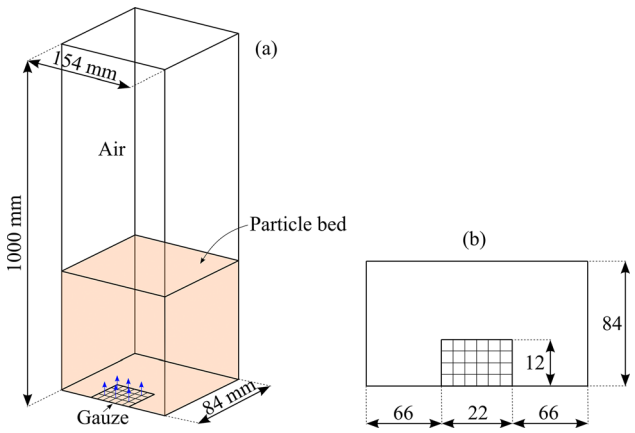

Fig. 2 **a** Schematic of the spout fluidised test setup and **b** configuration of the bed bottom with (meshed) gauze location

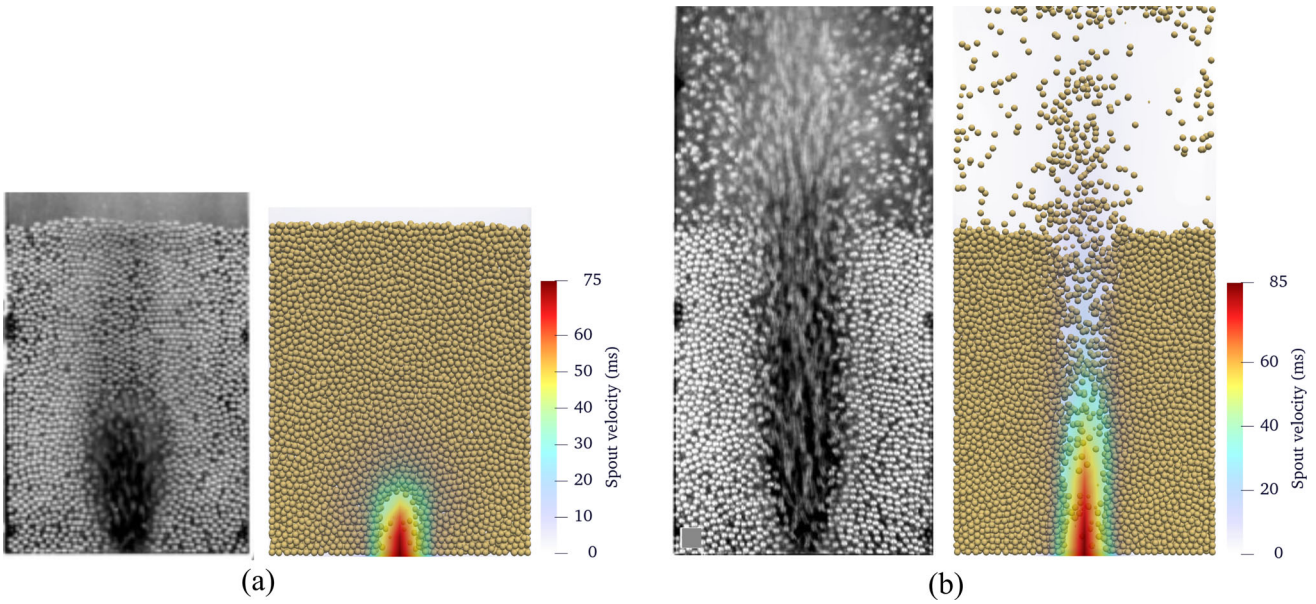

Fig. 3 Comparison of the simulation (bed section above the gauze) and experiment (adapted from Link et al. [17]) at the spouting velocity of **a** 75 m/s and **b** 85 m/s

channel has developed through part of the bed thickness and generated a small heave at the bed surface. The channel cross-sectional area is relatively the same as gauze area. As the spout channel continues to develop with increasing spout velocity, the particle bed finally becomes unstable with particles blowing up out of the bed surface. Figure 3b shows the particle beds at the spout velocity of 85 m/s with spout channel being developed throughout the entire bed thickness, resulting in bed fluidisation. Only particles in and close to the domain above the gauze are fluidised, while particles near the side walls remain stable. Such consistencies between the experimental and numerical results demonstrate the potentiality of the VOF-DEM method to capture the instability behaviour of dry particle beds subjected to fluid jet force. However, only two instances of the bed instability process could be compared due to the lack of relevant experimental results. It is still necessary that more detailed experiments of dry granular beds subjected to water jet should be conducted to provide concrete examples to further validate the VOF-DEM model in the future.

2.3 Application of the VOF-DEM model to investigate the instability of dry granular beds induced by water leakage

In this section, the VOF-DEM coupling method, which has been verified with the experiment above, will be employed to investigate the instability behaviour of dry granular beds subjected to water jet. The setup and numerical model of the granular bed test are illustrated in Fig. 4. Particles with

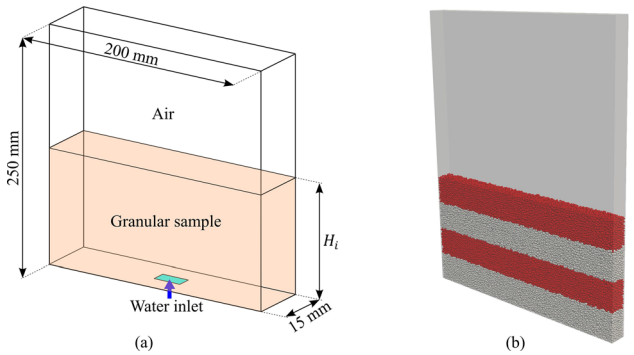

Fig. 4 **a** Schematic of the dry granular bed test setup; and **b** the numerical model

radii ranging from 0.8 to 1.2 mm (e.g. coarse sand commonly found in subgrade and capping layers under roads and railways) are randomly generated in a box domain of 200 × 250 × 15 mm and let to settle under gravity. Then, a vertical compaction load is applied through a wall at the bed top for particles to further distribute uniformly and avoid the formation of any weak area in the bed domain. This load is released before the application of water jet. The average void ratio of the particle assemblies is 0.62, which is comparable with sand with round or subround grain shapes [4]. The computational fluid domain has the same dimensions as the above box. At an initial stage before pipe leakage, this domain is assumed to consist of only air and dry soil particles. Upward water flow is then applied through an inlet located at the central of the domain's bottom boundary (i.e. the pipe-soil contact interface). Typical density and kinematic viscosity of air

Table 1 Model parameters of particles and fluid in the granular bed test

Particle (DEM)		Fluid (VOF)	
Property	Value	Property	Value
Young's modulus (GPa)	5	Water density (kg/m^3)	1000
Poisson's ratio	0.3	Air density (kg/m^3)	1
Coefficient of restitution	0.5	Surface tension coefficient (N/m)	0.07
Density (kg/m^3)	2000, 2500, 3000	Kinematic viscous coefficient of air (m^2/s)	10^{-5}
Sliding friction coefficient	0.2, 0.3, 0.4	Kinematic viscous coefficient of water (m^2/s)	10^{-6}
Rolling friction coefficient	0.15		

and water used in the simulations are given in Table 1, together with DEM particle properties. The no-slip velocity boundary is applied to the bottom, except the inlet, to represent the impermeable surface of the pipe. Atmospheric pressure is applied to the other boundaries of the fluid domain to let water drain freely towards all sides of the bed. During the simulation process, water inlet velocity is gradually increased until the granular bed is fully eroded. Three water inlet sizes are simulated in this study including 5 × 5 mm, 10 × 5 mm and 20 × 5 mm. For each inlet size, the behaviour of granular bed at three different bed thicknesses: 50, 100 and 150 mm, is investigated. The elastic properties of particles exhibit trivial effects on the bed behaviour, thus their typical values used in granular flow simulations are chosen. The base set of particle density ($\rho_p = 2500$ kg/m^3) and frictional properties with friction coefficient of 0.2 and rolling friction coefficient of 0.15 is obtained through calibration with experimental data of glass beads with same median particle size [16]. The values of particle density and friction coefficients are then varied as in Table 1 to assess their influences on the stability behaviour of dry granular beds. In total, thirteen simulations with different geometric and material parameters were conducted as summarised in Table 2.

3 Results and discussions

3.1 Instability mechanisms of dry granular bed

Under the effects of water jet force, the bed is eroded locally at the inlet while granular mass above is gradually bumped up. This process eventually leads to granular bed instability with the fluidilisation of granular mass in the area above the inlet. Similar to the instability process of saturated granular beds [32], dry granular beds exhibit three distinct regimes. Figure 5a–c typically shows the displacement of dry bed surface with the inlet size of 5 × 5 mm, 5 × 10 mm and 5 × 15 mm, respectively, indicating progressive changes in the bed behaviour with increasing water jet velocity. In the first regime, the jet velocity is still low and has negligible impacts on granular beds. The bed remains relatively static with no significant movement of particles, and there is no surface displacement in this regime. When water jet velocity is large enough, the granular mass starts to deform with heave formation on the bed surface–a common failure type of road formation. This also corresponds to the onset of the second regime. Throughout this regime, granular bed surface deforms at a constant rate with increasing the water jet velocity until reaching a critical value. The critical jet velocity is identified as the turning point from steady to unsteady bed deformation with a sudden increase in its surface deformation rate. It also signifies a transition from the second to third regime, i.e. fluidisation. In this final regime, granular mass above the inlet is quickly eroded, causing the bed surface to deform much faster than it does in the second regime. Particles in this area lose most of their contacts with each other, forming a fluidised zone in a triangular shape over the bed thickness.

Table 2 Summary of the parametric simulations of dry granular beds

ρ_p(kg/m^3)	μ	Bed height = 50 mm			Bed height = 100 mm			Bed height = 150 mm		
		5 × 5 inlet	5 × 10 inlet	5 × 15 inlet	5 × 5 inlet	5 × 10 inlet	5 × 15 inlet	5 × 5 inlet	5 × 10 inlet	5 × 15 inlet
2000	0.2				✔					
2500	0.2	✔	✔	✔	✔	✔	✔	✔	✔	✔
	0.3				✔					
	0.4				✔					
3000	0.2				✔					

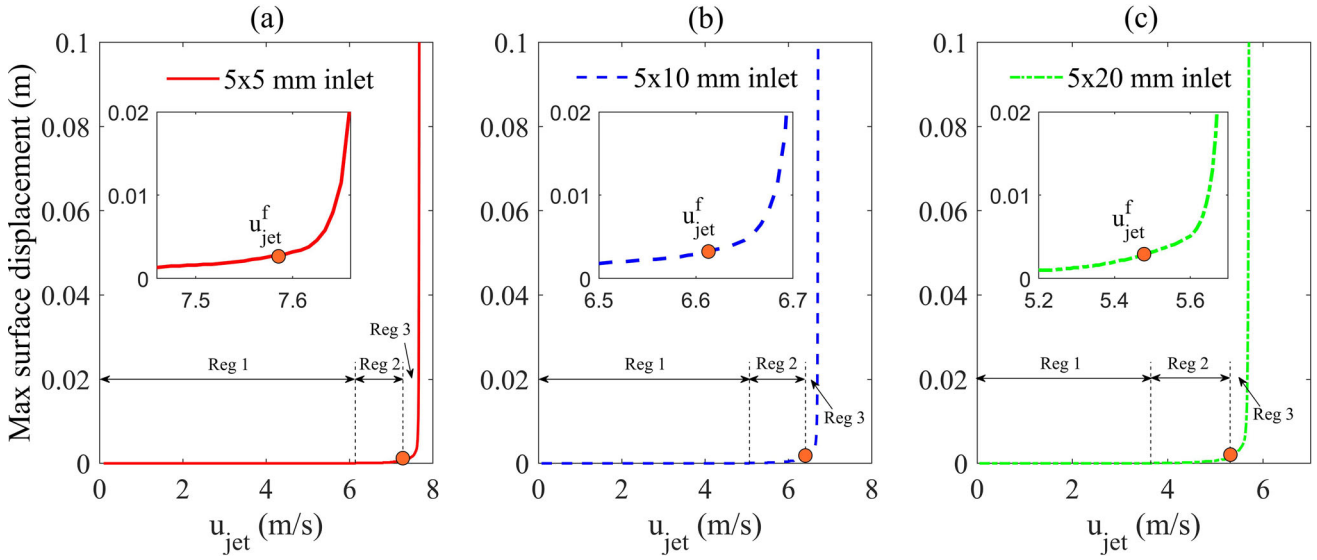

Fig. 5 Maximum vertical displacement of 100 mm bed surface with **a** 5 × 5 mm inlet, **b** 5 × 10 mm inlet and **c** 5 × 20 mm inlet, showing three regimes of the bed behaviour with respect to increasing water jet velocity. The insets show the graph zoom-in at the onset of the third regime with the orange dots representing critical jet velocities

Figure 6a–c shows the deformation process of granular beds with the bed thickness of 50, 100 and 150 mm, respectively, during the third regime. The granular beds are shown to deform significantly with small increases of water jet velocity. The fluidised zone of granular beds has a triangular shape with an open angle of 40^0 (or the coangle of 70^0). This value falls within the experimental range of saturated sand beds [9], which was reported to be 69 ± 3^0, but it is greater than those observed by Alsaydalani and Clayton [2]. This is attributed to different sizes and shapes of granular materials used in these studies. Both experiment and numerical results also show that the open angle is independent of granular bed thickness. The local failure of granular beds occurs right above the inlet where particles are completely washed out, eventually forming a vertical chimney similar to what observed for the saturated granular bed [9, 25]. Besides, the failure process is shown to deviate as granular bed thickness increases. For 50 and 100 mm beds (see Fig. 6a and b), the fluidised zone quickly extends to the bed surface when water jet velocity reaches the critical value. Nevertheless, for 150 mm granular bed (see Fig. 6c), local erosion first occurs right above the inlet, leading to the formation of a cavity in this area. This cavity gradually propagates upward as water jet velocity increases until the entire bed depth is fluidised.

To compare the behaviour of dry and saturated beds, simulations of saturated granular bed with the inlet size of 5 × 5 mm are performed. The setup and material properties used in this simulation are the same as those for the dry granular bed. The only difference is that the bed domain is now filled with water instead of air at the initial stage prior to pipe leakage. Results of the dry and saturated bed surface evolution and maximum displacement with increasing water jet velocity are presented in Fig. 7. The fluidised zone of the saturated bed is more localised than that of the dry bed (see Fig. 7a), and its open angle reduces from 40^0 to 32^0. The presence of water in granular beds loosen particle interactions, thereby reducing the resisting effective stress and narrowing down the mobilised area of saturated granular bed. Figure 7b compares the maximum surface displacement of dry and saturated bed as water jet velocity increases. While their failure regimes are quite similar, the saturated bed is shown to fail at a lower water jet velocity compared to the dry bed. The critical jet velocity at the onset of fluidisation of the dry granular bed is almost double of that of the saturated granular bed. This is understandable as the buoyant effect of water in the saturated granular bed reduces the gravitational force of granular mass, which is one of the main resistances to water jet force, by a factor of $\rho_s/(\rho_s - \rho_w)$.

3.2 Effects of granular bed thickness and water inlet size

The evolutions of bed surface displacement with different bed thicknesses when increasing water jet velocity are presented in Fig. 8a, showing clear effects of granular bed thickness on both the onset of bed surface deformation and fluidisation. The thicker the bed is, the larger water jet velocity is required to mobilise and fluidise granular mass. The values of water jet velocity at the onset of bed deformation (denoted by u^d_{jet}) and fluidisation (denoted by u^f_{jet}) are plotted in Fig. 8b. For various inlet areas, the

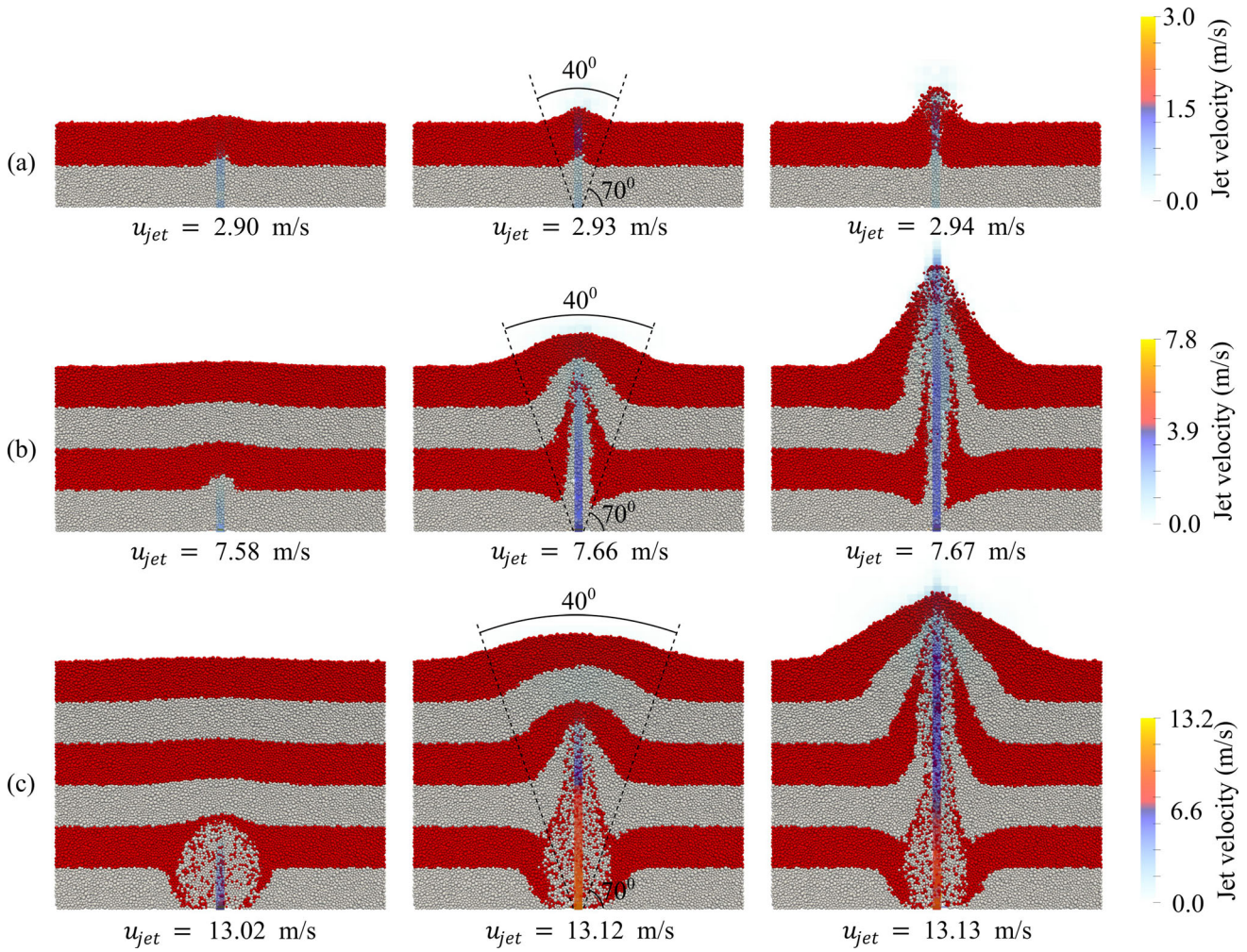

Fig. 6 Deformation process of dry granular bed with 5 × 5 mm inlet size and three different bed thicknesses: **a** 50 mm, **b** 100 mm and **c** 150 mm

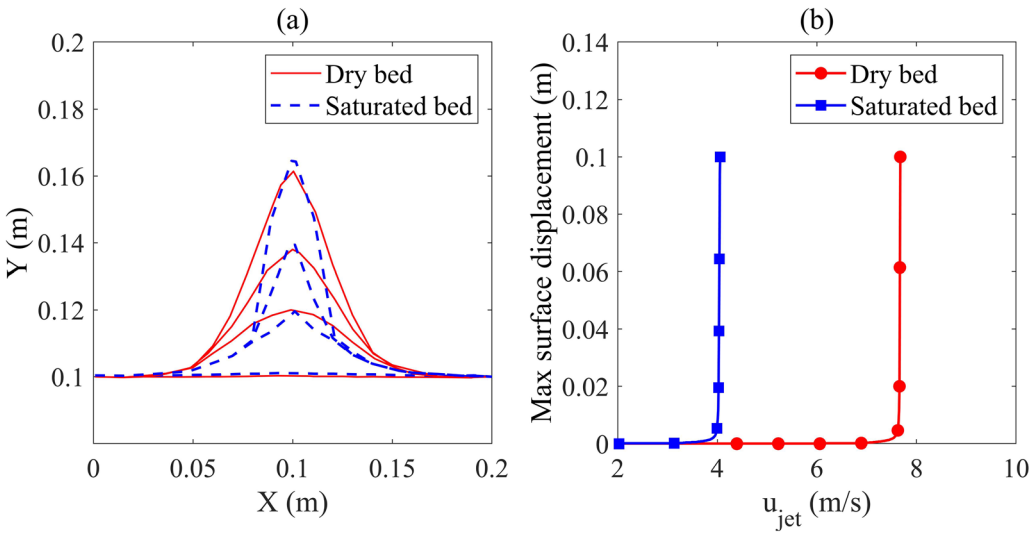

Fig. 7 Comparison of **a** the evolution of dry and saturated granular bed surface and **b** their maximum surface displacements when increasing water jet velocity. The compared granular bed is 100 mm thick, and the inlet size is 5 × 5 mm

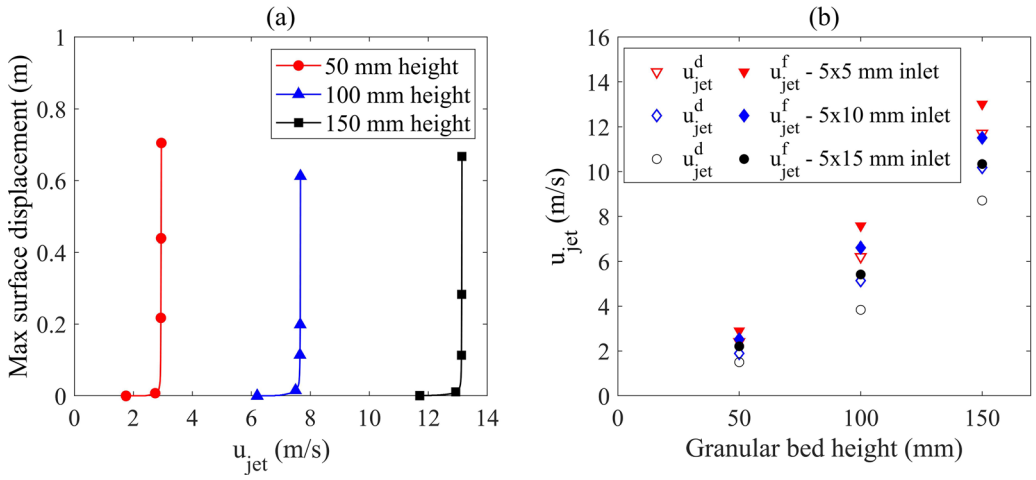

Fig. 8 **a** Maximum surface displacement of dry granular beds with different bed thicknesses and the inlet size of 5 × 5 mm when water jet velocity increases and **b** the results of water jet velocity at the onset of granular bed surface deformation (u_{jet}^{d}) and fluidisation (u_{jet}^{f})

increase of bed thickness results in larger u_{jet}^{d} and u_{jet}^{f}, similar to what observed for saturated beds [9, 25]. As the mobilised mass of granular bed increases with the bed thickness, it requires a larger upward driving force of water jet to win over the downward gravitational force of this mass. Besides, a thicker granular bed can effectively diffuse water jet force over the bed thickness, and hence water jet tends to induce local erosion near the inlet before propagating to the bed surface. In this case, soil particles around the water inlet region (i.e. pipe leakage) can migrate vastly under large hydrodynamic forces induced by high flow velocity, generating a cavity that gradually expands and eventually causes sudden collapse (e.g. sinkhole) of overlying infrastructures such as roads and railways. This process also corresponds to the extension of the second regime with steady deformation of granular bed surface when it becomes thicker as can be seen in Fig. 5 (Regime 2).

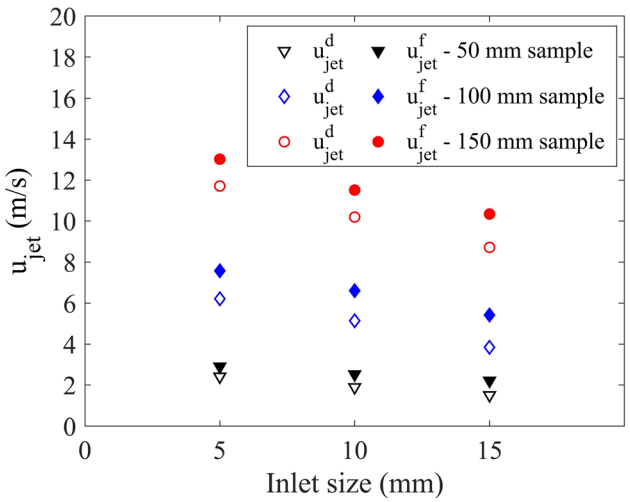

Fig. 9 The results of water jet velocity at the onset of granular bed surface deformation (u_{jet}^{d}) and fluidisation (u_{jet}^{f}) for different inlet sizes

The inlet size of water jet is shown to have inverse effects on the stability of granular beds. In particular, the values of both u_{jet}^{d} and u_{jet}^{f} of granular beds reduce with increasing inlet area as shown in Fig. 9. The same trend of critical jet velocity is also observed for saturated granular beds [20]. The reduction rate of u_{jet}^{d} and u_{jet}^{f} with respect to increasing inlet area tends to be higher for thicker beds, suggesting that the increase of buried depth would be more effective to improve dry granular bed stability if the defective area of pipes is expected to be small. The reduction of u_{jet}^{f} is not proportional to the increase of inlet area, which also indicates the instability assessment of dry granular beds against upward water jet should consider the jet velocity and inlet area (A_{in}) individually rather than their combination effect, i.e. the critical flow rate $Q^{c} = A_{in}u_{jet}^{f}$. On the other hand, the fluidised area and open angle of dry granular beds are shown to be almost independent of the inlet size, similar to those experimentally observed on saturated granular beds [26, 32].

3.3 Effects of granular material properties

Figure 10 presents the evolution of dry granular bed surface with different particle densities and frictional coefficients when increasing water jet velocity. It is noteworthy that the sliding friction angle of particles was varied from 0.2 to 0.4 to represent different morphologies such as shape and surface textures of soil particles in practice. Positive relationships between particle density or friction and the critical water jet velocity at the onset of granular bed fluidisation (u_{jet}^{f}) are observed. In particular, u_{jet}^{f} increases from 7.58 to 8.84 m/s when particle density increases from

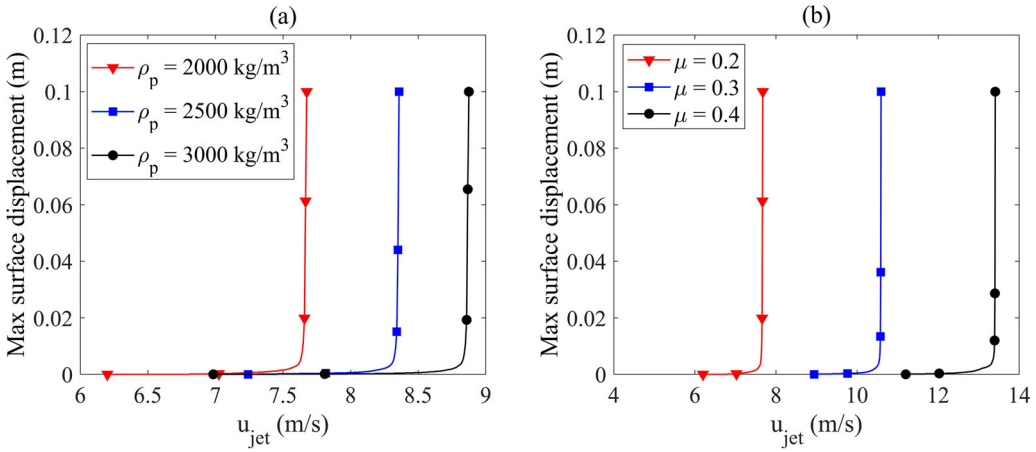

Fig. 10 Maximum surface displacement of dry granular beds with different values of **a** particle density and **b** friction coefficient when water jet velocity increases

2000 to 3000 kg/m^3 (corresponding to the bulk density varying from 1238 to 1857 kg/m^3), and u_{jet}^{f} increases from 7.58 to 13.37 m/s when the friction coefficient increases from 0.2 to 0.4. These results demonstrate the significant contributions of gravitational force (i.e. self-weight) and frictional force exerted in dry granular beds to resist the driving force of upward water jet. The contribution of gravitational force to bed resistance is intuitively reasonable given its opposite direction to the water jet force, whereas frictional resisting force acts on the sliding planes between the mobilised and static bodies of the particle bed tends to increase as the material friction angle increases as per Mohr–Coulomb failure criterion. On the other hand, the mobilised mass of dry granular beds is shown to be almost constant as its open angle remains around 40 ± 1^0 regardless of various values of particle density and friction coefficient. Such observation is interesting as the open angle is also demonstrated above to not depend on the dry granular bed thickness and inlet size. This would make any future attempts to develop (semi-)analytical solutions to determine the critical jet velocity causing dry bed instability become less strenuous.

4 Conclusion

This study employs a VOF-DEM coupling method to numerically investigate the stability behaviour of dry granular beds due to water pipe leakage. The numerical model is first validated with experimental data of a dry spout fluidised bed and is then applied to simulate the plane-strain setup of dry granular beds subjected to upward water jet resulted from pipe leakage. Based on the numerical results, following conclusions can be made:

- Under the effects of increasing water jet velocity, dry granular beds exhibited three different regimes, i.e. stationary, constant deformation (heave) and fluidisation, similar to the behaviour of saturated granular beds observed in previous experimental studies. However, the current study found that the dry beds can encounter a larger water jet force (or larger jet velocity), while experiencing larger fluidised zones compared to saturated beds. Such distinctions highlight a necessity for more research on the behaviour of dry granular beds as knowledge of saturated beds is not directly applicable.
- The instability mechanism of dry beds was influenced by both the bed thickness and water inlet size. Water jet velocity at the onset of deformation and fluidisation of the beds were shown to increase with thicker bed and smaller inlet area. Increasing bed thickness also accelerated the localised erosion of granular mass around the water inlet, leading to cavity formation prior to full-depth fluidisation of the granular bed.
- The gravitational and frictional forces were two main resisting factors of dry granular beds against the driving force of water jet. This study proved that increasing particle density and friction coefficient of dry bed material can significantly enhance the bed resistance to water jet-induced failures, i.e. larger values of u_{jet}^{d} and u_{jet}^{f}. The open angle of the mobilised zone in dry granular beds, on the other hand, was found to be almost independent of the bed thickness.

These findings can provide useful references to important factors that need to be considered in the stability assessment of dry granular beds. However, we acknowledge that this study could not cover all important aspects of the problem, especially given a bare lack of experimental data. Therefore, it is suggested to conduct more experiments to confirm the instability mechanisms of physical

granular bed (e.g. sands, gravels) and provide references for further validations of numerical models. In addition, the effects of overburden loads, consolidation and saturation degree should be characterised to provide more comprehensive understanding of the problem.

Acknowledgement Funding support by the internal grant at the School of Engineering, Deakin University (PRESS2023), is gratefully acknowledged.

Funding Open Access funding enabled and organized by CAUL and its Member Institutions.

References

1. Ai J, Chen J-F, Rotter JM, Ooi JY (2011) Assessment of rolling resistance models in discrete element simulations. Powder Technol 206:269–282. https://doi.org/10.1016/j.powtec.2010.09.030
2. Alsaydalani MOA, Clayton CRI (2014) Internal fluidization in granular soils. J Geotech Geoenviron Eng 140:04013024
3. Brackbill JU, Kothe DB, Zemach C (1992) A continuum method for modeling surface tension. J Comput Phys 100:335–354. https://doi.org/10.1016/0021-9991(92)90240-Y
4. Cubrinovski M, Ishihara K (2002) Maximum and minimum void ratio characteristics of sands. Soils Found 42:65–78
5. Cui X, Li J, Chan A, Chapman D (2012) A 2D DEM–LBM study on soil behaviour due to locally injected fluid. Particuology 10:242–252
6. Di Renzo A, Di Maio FP (2004) Comparison of contact-force models for the simulation of collisions in DEM-based granular flow codes. Chem Eng Sci 59:525–541. https://doi.org/10.1016/j.ces.2003.09.037
7. Galindo-Torres SA (2013) A coupled Discrete Element Lattice Boltzmann Method for the simulation of fluid–solid interaction with particles of general shapes. Comput Methods Appl Mech Eng 265:107–119
8. Goniva C, Kloss C, Deen NG, Kuipers JAM, Pirker S (2012) Influence of rolling friction on single spout fluidized bed simulation. Particuology 10:582–591
9. He Y, Zhu DZ, Zhang T, Shao Y, Yu T (2017) Experimental observations on the initiation of sand-bed erosion by an upward water jet. J Hydraul Eng 143:06017007
10. Hertz H (1882) Über die Berührung fester elastischer Körper. J für die reine und angewandte Mathematik 92:22
11. Jiang L-J, Zhang B, Huang S-H, Shao Y (2023) Analysis of fluidized zone in transparent soil under jet induced by pipe leakage. Water Sci Eng (In press). https://doi.org/10.1016/j.wse.2023.01.002
12. Karimi H, Dehkordi AM (2015) Prediction of equilibrium mixing state in binary particle spouted beds: effects of solids density and diameter differences, gas velocity, and bed aspect ratio. Adv Powder Technol 26:1371–1382
13. Kloss C, Goniva C, Hager A, Amberger S, Pirker S (2012) Models, algorithms and validation for opensource DEM and CFD–DEM. Progr Comput Fluid Dyn, an Int J 12:140–152
14. Koch DL, Hill RJ (2001) Inertial effects in suspension and porous-media flows. Annu Rev Fluid Mech 33:619–647
15. Lai Z, Zhao J, Zhao S, Huang L (2023) Signed distance field enhanced fully resolved CFD-DEM for simulation of granular flows involving multiphase fluids and irregularly shaped particles. Comput Methods Appl Mech Eng 414:116195
16. Li P, Wang D, Wu Y, Niu Z (2021) Experimental study on the collapse of wet granular column in the pendular state. Powder Technol 393:357–367
17. Link JM, Cuypers LA, Deen NG, Kuipers JAM (2005) Flow regimes in a spout–fluid bed: A combined experimental and simulation study. Chem Eng Sci 60:3425–3442
18. S. McPhee (2019) Back wheels of Sydney bus stuck in sinkhole after water main burst. News.com.au Available at: https://www.news.com.au/national/nsw-act/news/back-wheels-of-sydney-bus-stuck-in-sinkhole-after-water-main-burst/news-story/93cc64a978cc1efb6be3705c32311c3d.
19. Mindlin RD, Deresiewicz H (1953) Elastic spheres in contact under varying oblique forces. J Appl Mech 20(3):327–344
20. Ngoma J, Philippe P, Bonelli S, Radjaï F, Delenne J-Y (2018) Two-dimensional numerical simulation of chimney fluidization in a granular medium using a combination of discrete element and lattice Boltzmann methods. Phys Rev E 97:052902
21. Nguyen NHT (2022) Collapse of partially and fully submerged granular column generating impulse waves: an empirical law of maximum wave amplitude based on coupled multiphase fluid–particle modeling results. Phys Fluids 34:013310
22. Nguyen NHT, Nguyen TT, Phan QT (2022) Dynamics and runout distance of saturated particle-fluid mixture flow on a horizontal plane: A coupled VOF-DEM study. Powder Technol 408:117759
23. Shen Z, Wang G, Huang D, Jin F (2022) A resolved CFD-DEM coupling model for modeling two-phase fluids interaction with irregularly shaped particles. J Comput Phys 448:110695
24. S. Steger (2020) Huge sinkhole swallows car in Bennett Springs as driver escapes uninjured. The West Australian Available at: https://www.perthnow.com.au/news/disaster-and-emergency/huge-sinkhole-swallows-car-in-bennett-springs-as-driver-escapes-uninjured-ng-b881604488z.
25. Tang Y, Chan DH, Zhu DZ (2017) Numerical investigation of sand-bed erosion by an upward water jet. J Eng Mech 143:04017104
26. J.E. Van Zyl, M.O.A. Alsaydalani, C.R.I. Clayton, T. Bird, A. Dennis, (2013) Soil fluidisation outside leaks in water distribution pipes–preliminary observations, Thomas Telford Ltd, pp. 546–555.
27. Vångö M, Pirker S, Lichtenegger T (2018) Unresolved CFD–DEM modeling of multiphase flow in densely packed particle beds. Appl Math Model 56:501–516. https://doi.org/10.1016/j.apm.2017.12.008
28. Yang S, Sun Y, Zhang L, Zhao Y, Chew JW (2016) Numerical investigation on the effect of draft plates on spouting stability and gas–solid characteristics in a spout-fluid bed. Chem Eng Sci 148:108–125
29. Zhao J, Shan T (2013) Coupled CFD–DEM simulation of fluid–particle interaction in geomechanics. Powder Technol 239:248–258

30. Zhong W, Yu A, Liu X, Tong Z, Zhang H (2016) DEM/CFD-DEM modelling of non-spherical particulate systems: theoretical developments and applications. Powder Technol 302:108–152
31. Zhou YC, Wright BD, Yang RY, Xu BH, Yu AB (1999) Rolling friction in the dynamic simulation of sandpile formation. Phys A 269:536–553. https://doi.org/10.1016/S0378-4371(99)00183-1
32. Zoueshtiagh F, Merlen A (2007) Effect of a vertically flowing water jet underneath a granular bed. Phys Rev E 75:056313